When probabilistic seismic hazard climbs volcanoes: the Mt Etna case, Italy. Part I: model components for sources parametrization

Raffaele Azzaro[1], Graziella Barberi[1], Salvatore D'Amico[1], Bruno Pace[2], Laura Peruzza[3], Tiziana Tuvè[1]

[1]Istituto Nazionale di Geofisica e Vulcanologia (INGV), Sezione di Catania – Osservatorio Etneo, 95123, Italy
[2] DiSPUTer, Università "G. d'Annunzio" Chieti-Pescara Via dei Vestini, Chieti, Italy
[3]Istituto Nazionale di Oceanografia e di Geofisica Sperimentale – OGS, Sgonico (TS), 34010, Italy

Correspondence to: Raffaele Azzaro (raffaele.azzaro@ingv.it)

Abstract. The volcanic region of Mt Etna (Sicily, Italy) represents a perfect lab for testing innovative approaches to seismic hazard assessment, given the availability of a long record of historical and recent observations of seismic and tectonic phenomena, the high quality of various geophysical monitorings and especially because the very fast geodynamics clearly demonstrate some seismotectonic processes. We present here the model components and the procedures adopted for defining seismic sources to be used in a new generation of Probabilistic Seismic Hazard Assessment (PSHA) whose first results and maps are presented in a companion paper, Peruzza et al. (2017). The sources include, in a picture of increasing complexity, area seismic zones, individual faults and gridded point sources that are obtained by integrating geological field data with long and short earthquake datasets (the historical macroseismic catalogue that covers about three centuries, and a high-quality instrumental locations database for the last decades). The analysis of the frequency-magnitude distribution identifies two main fault systems within the volcanic complex featuring different seismic rates that are controlled essentially by volcano-tectonic processes. We discuss the variability of the mean occurrence times of major earthquakes along the main Etnean faults by using an historical approach and a purely geologic method. We derive a magnitude-size scaling relationship specific for this volcanic area, which was has been implemented into a recently developed software tool – *FiSH,* Pace et al. (2015) – which we use to calculate the characteristic magnitudes and the related mean recurrence times expected for each fault. Results suggest that for Mt Etna area, the traditional assumptions of uniform and Poissonian seismicity can be relaxed; a time-dependent fault-based modelling, joined with a 3D imaging of volcano-tectonic sources depicted by the recent instrumental seismicity, can be therefore implemented in PSHA maps. They can be relevant for the retrofitting of the existing building stock, and for driving risk reduction interventions. These analyses do not account regional M>6 seismogenic sources which dominate the hazard at long exposure times (≥50 yrs).

1 Introduction

Mt Etna, the largest active volcano in Europe, is commonly known for striking volcanic phenomena, featuring nearly constant summit activity and frequent flank eruptions. However, apparently less evident but equally impressive are tectonic phenomena occurring along the eastern and southern slopes of the volcano, which are crossed by different systems of active

faults (Azzaro et al., 2012a). The most severe effect of this tectonic activity is the intense seismicity shaking the urbanised areas of the volcano, with obvious implications arising in terms of seismic hazard.

For this reason one of the goals the DPC-INGV V3 Project on the "multi-disciplinary analysis of the relationships between tectonic structures and volcanic activity" (Azzaro and De Rosa, 2016a, 2016b) was to assess seismic hazard in the eastern

35 flank of Etna due to local volcano-tectonic earthquakes. Taking advantage of the huge amount of geological, seismological and geodetic data which derive from field observations and multi-parametric monitoring, we had the opportunity to test innovative methodological approaches and computation codes developed for the whole Italy in the framework of companion projects (Peruzza, 2013), adapting them to consider the features of the volcano-tectonic seismicity. In practise this meant analysing large seismological and geological datasets to parameterise the seismicity rates of seismic sources and hence the

40 earthquake occurrence probability, thus improving the results of previous researches based solely on the use of macroseismic intensity data (Azzaro et al., 2013b, and references therein).

In this study we present the application of the entire procedure to characterise seismic sources at Etna with an increasing degree of detail and complexity providing, for the first time on this volcano, a comprehensive view of the seismotectonic features and an analytical estimation of input parameters, with related uncertainties, for seismic hazard purposes. We

45 integrated historical and instrumental earthquake catalogues to define four seismic zones around the main fault systems recognised in the area, identifying the seismogenic layers where most of the seismic energy is released (effective depth) and estimating seismic rates through the frequency-magnitude distribution (FMD). We also used a distributed seismicity model for describing background earthquakes in the crustal volume beneath Etna by adopting a high resolution three-dimensional grid (inter-nodal distance of 2 km). In addition we performed the characterisation of the sources at the scale of the individual

50 faults by applying a purely geological approach (Pace et al., 2015) that considers the geometric-kinematic parameters representative of fault activity (dimensions and slip-rate). To this end we first obtained a magnitude-size scaling relationship specific for this volcanic region and then calculated the seismic rates expressed in terms of mean recurrence time of the maximum magnitude expected on each fault.

The obtained dataset defines the input parameters used in a full Probabilistic Seismic Hazard Assessment (PSHA) at a local

55 scale of Etna, discussed in a companion paper (Peruzza et al. 2017, hereinafter referred as Part II). Finally, we remark that the amount of multi-disciplinary data used here for source parametrization as well as the consistency of results represent, in our opinion, an unique condition compared to both other volcanic districts worldwide and tectonic areas. In this sense, we hope that this work can be regarded as a case study for improving methodological approaches and conceptual procedures in fault-based, time-dependent hazard estimations.

60 2 Linking faults to earthquakes at Mt Etna: a short overview

Mt Etna volcano is an ideal lab for observing at a small-scale a full range of faulting processes that in other regions is difficult to find taking place all together. Evidence of active tectonics is impressive and widespread particularly in the

eastern flank, where morpho-tectonic features (Azzaro et al., 2012a), recurrent seismicity (presented extensively in Sections 3 and 4) and ground deformations (Bonforte et al., 2011; Bruno et al., 2012) provide a real measure of the intense volcano-

65   tectonic activity. Furthermore, a more than centennial documented history of surface faulting related to coseismic displacements (Azzaro, 1999) and creeping phenomena (Rasà et al., 1996) suggests a clear picture of the relationship between faults and earthquakes; the long list of large and minor events rupturing different segments of the same faults (Fig. 1a) has led to a detailed mapping of active faults and characterisation of their behaviour both in the long- and short-term (Azzaro et al., 2013a).

70   All these features allowed us to constrain a seismotectonic model (Azzaro, 2004) where faults slip in a strongly heterogeneous mode along strike, with two end-member rupture mechanisms addressing fault segments ruled by stick-slip behaviour (earthquake-related slip) or by stable-sliding behaviour (aseismic creeping) (Fig. 1b). In this framework the Timpe system and the Pernicana fault represent the most important tectonic elements at Etna, dissecting the eastern flank between the coast and the volcano-tectonic structures of the NE Rift and Valle del Bove depression (Azzaro et al., 2012a, 2013a and

75   references therein). They both appear very active from a seismotectonic point of view, in terms of the number of earthquakes and maximum magnitudes. While the long-term seismic history of the Pernicana fault is limited to few decades – the urbanisation of the uphill sector crossed by the fault dates back to the late 1970s – the Timpe system is the area responsible for most of the strongest earthquakes known to have occurred at Etna since early 1800s: from a total of twelve largest events – here we consider those having epicentral intensities I_0 larger than degree VIII EMS, i.e. producing at least severe damage

80   according to the European Macroseismic Scale (see Grünthal, 1998) – ten of them are located here, determining this densely inhabited zone of Etna as the most hazardous of the volcano (Azzaro et al., 2016).

Finally a debated issue in modelling seismic sources of volcanic regions for seismic hazard applications regards the question of whether fault behaviour is controlled by the volcanic activity *stricto sensu*. It is a matter of fact that destructive earthquakes in the Timpe area historically occurred both during flank eruptions and not; correlation studies of major seismic

85   events and volcanic activity have not produced univocal results (Gasperini et al., 1990; Nercessian et al., 1991; Gresta et al., 1994). Conversely, analyses based on the integration of long time series of geodetic data and seismic data (Bruno et al., 2012; Solaro et al., 2010; Bozzano et al., 2013; Palano, 2016 and references therein) highlighted the main role of large-scale instability processes in governing the dynamics of the lower eastern flank of Mt Etna, where strain behaves as steady process on a decennial time scale (Bonforte et al., 2011). In this picture it has to be stressed that the mode of seismic release in a

90   wide area encompassing the Timpe system, which is indeed a structurally homogeneous domain of characterised by a general east-west extension (Bousquet and Lanzafame, 2004), features an intertime distribution of earthquakes more similar to a tectonic style rather than a volcanic one (see also Traversa and Grasso, 2010; Sicali et al., 2014). We therefore accept that these faults are constantly (on average) loaded in time as expected in a typical tectonic process.

3 Historical seismicity: some hints for long-term fault behaviour

95 Information provided from macroseismic data is representative of the long-term seismicity since the effects of past major earthquakes affecting the urbanised areas of the volcano are well documented (Azzaro et al., 2000; Azzaro and Castelli, 2015). The historical earthquake dataset used for the analysis is the CMTE catalogue (CMTE Working Group, 2017), covering the time-span 1600-2013 and including fore- and aftershocks also of low intensity; overall, nearly 1,800 events are listed in the catalogue. The magnitude of completeness of this macroseismic catalogue has been estimated as M_c 3.7: it

100 corresponds to an epicentral intensity I_0 VII EMS (i.e. moderate damage), according to the relationship derived by Azzaro et al. (2011).

For our analysis we selected the historical earthquakes located along the Timpe fault system (Fig. 2), limiting our attention to the strongest events with I_0 ranging from VIII to IX-X EMS (i.e. from severe damage up to destruction) and with a moment magnitude M_W from 4.6 to 5.2 (Azzaro et al., 2011). It has to be noted that moderate values of magnitude for heavily

105 damaging events are a feature of seismicity in active volcanic areas such as Etna, whereas in tectonic domains crustal earthquakes producing the same effects are generally associated with M~>6. The final dataset therefore covers the time-span 1805-2015 and consists of nine earthquakes, whose causative faults are clearly recognised through extensive evidence of coseismic surface faulting (Azzaro, 1999). Earthquakes and associated faults used in the analysis are indicated in Figs. 1 and 2. Thus, the long-term mean recurrence time of historical major events in the Timpe area, reconstructed over a period of 210

110 years by the fault seismic histories (see Azzaro et al., 2013b), is just 23 years.

3.1 Characteristic magnitude and mean recurrence times by historical approach

Supported by the observation that major earthquakes have produced surface faulting ruptures along strike for the entire or most of the length of their causative faults (Azzaro, 1999), we assume that seismogenic Timpe faults behave according to the characteristic earthquake model (*sensu* Schwartz and Coppersmith, 1984). The earthquake size beyond which the

115 phenomenon becomes evident corresponds to events having $I_0 \geq$ VIII EMS, equivalent to $M_W \geq 4.6$. These characteristic earthquakes therefore represent the maximum or quasi-maximum historically observed events: in Section 5.3 we will face the problem of maximum potential earthquake on faults by means of magnitude-size vs fault dimension relationships.

In previous studies we have calculated the mean recurrence time (T_{mean}) of a characteristic earthquake by simple intertimes statistics, given by the sum of all the inter-event times of major events divided by the number of the intertimes (see details in

120 Azzaro et al., 2012b). We considered two cases: i) events occurring everywhere inside the SZ Timpe, ii) events occurring at the scale of individual faults. In the first case, with eight intertimes available, we obtained a T_{mean} of 24.6 years (with a standard deviation $\sigma = 21.4$ years), a value very similar to the one obtained from the historical rate (23 years) that accounts of open intervals too; the aperiodicity factor α (obtained by $\sigma/T_{mean} = 0.87$) is typical of a quasi Poissonian process. In the second case we calculated intertimes of earthquakes occurring on the same fault (six intertimes), then, summing them

125 together, we applied statistics: T_{mean} rises to 71.3 years and α drops to 0.42, a typical value for semi-periodic processes. In

the inset of Fig. 2, the probability of having a characteristic earthquake on an individual fault is given according to a Poisson distribution (horizontal pink line at about 7% in 5 years, time invariant) and a Brownian Passage Time distribution (coloured "waves" in which the occurrence time of earthquakes assigned to each fault is represented by the sharp drop of the conditional probability function); note that all the historical events have occurred when the time-dependent probability of

130 having an earthquake in the next 5 years is higher than the one derived with stationary assumptions, thus supporting the choice of time-dependency in our analysis. By doing this, we of course consider that fault behaviour inside SZ Timpe is somehow uniform being affected by the same seismotectonic regime (Alparone et al., 2011). Since the intertimes dataset is not robust from a statistical point of view, similarly to the procedure adopted for paleoseismic datasets (Parsons, 2008) we also applied a bootstrap analysis to verify the confidence intervals of the results: T_{mean} remains stable while α is 15% lower

135 than the previously reported values.

4 Recent earthquake dataset: from the instrumental catalogue to the characterisation of seismic sources

Regarding the short-term seismicity, we used data recorded by the seismic network of eastern Sicily that is operated by the Istituto Nazionale di Geofisica e Vulcanologia, Osservatorio Etneo, in Catania. Although the instrumental data at Etna have been collected since early 1990s, a revised and complete earthquake catalogue has been compiled since 2000 by using a

140 one-dimensional V_P velocity model (Alparone et al., 2015; Gruppo Analisi Dati Sismici, 2016). For the purposes of this study, we considered only the portion of the catalogue from 2005 to 2015 because in this time-window the seismic rate appears generally regular, not altered by the significant steps typically related with the seismic swarms accompanying eruptions at Etna, as occurred in 2001 and 2002-03 (Fig. 3). Moreover, since 2005 the seismic network has undergone a relevant upgrade, both in the number of stations and technology, with broad band 3-component seismometers and digital

145 acquisition. This technological development has allowed the detection of very low energy events (magnitude ≤ 1), the calculation of homogeneous and well calibrated local magnitudes (Tuvè et al., 2015) and the application of advanced techniques for locating hypocentres (Mostaccio et al., 2013).

In order to better define seismic clusters or hypocentral alignments, thus contributing to the seismic source identification needed by the V3 Project, the 2005-2015 earthquake dataset was re-processed (Cocina et al., 2016) by using a three-

150 dimensional V_P velocity model (Alparone et al., 2012) and the tomoDDPS algorithm (Zhang et al., 2009). Compared to more simple methods, this code uses a combination of both absolute and differential arrival time readings between events of an earthquake cluster, so that for earthquakes with foci lying close to each other, travel time errors due to incorrect velocity models in the volume outside the cluster, are essentially cancelled out.

As a result, we obtained a revised dataset consisting of 4,286 seismic events with M_W up to 4.8; the magnitude of

155 completeness of the catalogue M_c is 1.1. Regarding the magnitude scale, the M_W values of major recent earthquakes are taken from the literature or MedNet bulletin (http://mednet.rm.ingv.it/earthquakes.php), whereas we adopted the M_L-M_W relationship calibrated on moment tensor analysis (Saraò et al., 2016) to convert the M_L values reported in the catalogue. In

general, most of shallowest earthquakes occurring at Etna in the time-span 2005-2015 are located in the eastern sector of the volcano within 7 km of depth (orange in Fig. 4a), clustering around the tectonic features of the Timpe and Pernicana fault systems. It should be stressed that this seismicity is strictly related with the continuous fault activity and volcano-tectonic dynamics as a whole (Patanè et al., 2004; Solaro et al., 2010). Conversely, seismicity occurring at deeper crustal levels mainly represents purely-tectonic regional dynamics due to the current compressive regime at the front of the Sicilian Chain-Foreland (La Vecchia et al., 2007; De Guidi et al., 2015; Scarfi et al., 2016). The most significant seismogenic volume in the deep crust beneath Etna is the one in the north-western sector of the volcano, with focal depths in the range of 22- 30 km.

4.1 Area seismic sources

The area sources represent the most simplified representation of the fault systems relevant for seismic hazard. Area sources, or seismogenic zones (hereinafter SZ), are polygons including one or more faults where the earthquake occurrence rate is uniformly distributed and seismicity occurs at a defined (i.e. fixed) level of depth. This conceptual approach has been used in the past for the Italian seismic hazard map MPS04 (Meletti et al., 2008; Stucchi et al., 2011) and, more recently, for the global hazard map in the SHARE project too (Woessner et al., 2015).

Despite the detailed knowledge of the geometries of the active faults at Etna (Azzaro et al., 2013a), the definition of a SZ is not an easy task since the individual tectonic elements here considered are very close to each other, even 1 km apart in the case of the Timpe fault system (Azzaro et al., 2012a). The borders of the SZs are then defined by the spatial distribution of the relocated instrumental earthquake dataset considering only the shallowest events occurring within 7 km depth (orange in Fig. 4a). This is in agreement with the superficial nature of the volcano-tectonic structures, not rooted in the crust. In addition, we considered a buffer around the fault lines and grouped adjacent structures. In this way we obtained four areal seismic sources – three for the Timpe system and one for the Pernicana system (blue polygons in Fig. 4a) – respecting the homogeneity in terms of other seismological and geological features (M_{max}, length and width, kinematics, slip-rate, see also De Guidi et al., 2012).

These SZs represent the recent seismotectonic activity of the shallowest crust (≤7 km) at Mt Etna and also include the sources of the strongest historical earthquakes ($M_W \geq 4.6$) discussed before. The number of earthquakes used for the detailed characterisation of the areal sources, are about 1,000. Moreover, we also considered an extended SZ embracing the whole Timpe system, shown as red polygon in Fig. 4a. This option has a dual purpose: i) to provide a less detailed characterization mediating features inside heterogeneous, ii) to assess the uncertainty associated with the geometry of the sources and hence to explore the variability of the parameters used in the hazard computation.

4.1.1 Effective depth

The characterization of the area sources includes the estimation of the effective depth, i.e. the seismogenic layer where most of the seismic energy is released. For this purpose we calculated, by using the events included in each SZ, the distribution of the number of earthquakes above the completeness threshold and the related strain release vs. the focal depth, with steps of 1

190 km. Results in Fig. 5 indicate that the seismogenic thickness is mainly confined to the first 5 km of crust, a value in agreement with the focal depth distribution of overall seismicity in the Etna region (Fig. 4b). Note that, due to the cone-shaped topography of the volcano rising up 3000 m, hypocenters can be located above sea level (depth in these cases assumes negative values). Looking in more detail, a first seismogenic layer can be observed at 0-2 km below sea level (bsl) in all SZs, but also a second layer is evident at 4-5 km bsl defining the bottom of STF-SVF and MF-SLF area sources. It

195 must be stressed that major seismicity (M ≥ 3.0 eqs.) occurs within both the layers (dark blue in Fig. 5). A similar pattern also emerges for the Timpe SZ, which includes the aforementioned individual SZs (except PF), confirming the main contribution to seismogenesis of the deeper focal depth level. In conclusion, SZs at Etna are characterized by shallow effective depths, with PF and FF in the range 0 to 2 km and other sources between 0 to 5 km bsl (marked by orange stripes in Fig. 5). These intervals are used as reference depths in the hazard computation (see details in Peruzza et al., 2017).

200 **4.1.2 Seismic rate**

Seismic rates have been determined by analysing the frequency-magnitude distribution from the instrumental earthquake catalogue by using the ZMap tools (Wiemer, 2001). The FMD of each SZ is estimated by maximum likelihood method (Wiemer and Wyss, 2002) using only the shallowest events (those occurring within a depth of 7 km bsl), so that a and b coefficients of the Gutenberg-Richter (GR) relationship are representative of the seismic activity of shallow sources. The

205 magnitude of completeness M_c of this subset of data is 1.3-1.4. The obtained FMDs (red in Fig. 6) indicate that the Timpe faults (FF, STF-SVF, MF-SLF) have b-values varying from 0.84 to 1.13 (Tab. 1), while the Pernicana fault (PF) it is characterized by a lower b-value (0.64).

In order to check if the FMDs obtained from an instrumental earthquake dataset during an interseismic period of just 11 years can be representative of the deformation processes driving the volcano-tectonic activity on the flanks of Mt Etna, and

210 thus adequate for describing the long-term seismogenic behaviour, we calculated FMDs from the historical macroseismic catalogue (blue symbols in Fig. 6). The historical catalogue covers a time-span of ca. 150 years for all the SZs except for PF, whose anthropisation (and thus the seismic history) is limited to the last decades at most. Since the time extension of the instrumental and historical sub-catalogues is different, all the FMDs are represented after a normalization to one year. The visual comparison of the observed rates shows a satisfying agreement between macroseismic and instrumental data; no jump,

215 or huge variations in slope exist, as often happens when dealing with such analyses, for example due to non-uniform magnitude assessment. For the Timpe sources (treated as a group, or separated in main fault systems in FF, STF-SVF, MF-SLF) the macroseismic FMDs are within the uncertainties of the instrumental ones, starting approximately above M_W 3.5. Above this point, historical data represent the GR relationships for the high magnitudes, obviously not represented during an interseismic phase; conversely, the macroseismic FMDs deviate from the GR fitting at low magnitudes, thus representing the

220 incompleteness of historical records for small earthquakes, a fact that it is widely known. Regarding the PF, the minor fit of instrumental and macroseismic FMDs is certainly due to the incompleteness of the macroseismic catalogue (short seismic

history and events 'lost' because the area is hardly urbanized). Finally, we calculated α from GR according to Zöller et al. (2008) (see Tab. 2).

In conclusion, since we believe that the FMDs from instrumental and historical macroseismic catalogues are sufficiently
225 consistent with each other, we accept the simplification of adopting the 2005-2015 instrumental seismicity rates as proxies for the long-term seismogenic behaviour of area sources. Therefore *a* and *b*-values are calculated from the instrumental seismicity detected by high-quality monitoring during an interseismic period (i.e. in which no seismic swarm due to eruptions or volcanic activity has significantly affected our SZs) and will be used for characterizing the seismicity rates and extrapolating the GRs beyond the maximum value observed in these 11 years. The maximum magnitude has to be fixed on
230 independent criteria which will be historical and/or geological, as described in the following.

4.2 Distributed seismicity

An alternative gridded seismicity approach has been used to depict 3D point sources in a crustal volume beneath Mt Etna. We calculated the *a*- and *b*-values of the GR relationship as follows: we created a three-dimensional grid with an inter-nodal distance of 2 km and applied a constant search radius of 3 km to sample the 2005-2015 instrumental earthquake dataset; grid
235 nodes with less than 20 earthquakes were discarded. The maximum-likelihood method according to Wiemer and Wyss (2002) was applied for GR interpolation of events above the M_c threshold (1.3); *a*-values have been normalized according to the volume represented. In this way we obtained a grid consisting of 422 nodes; however, since the obtained sample of *a*- and *b*-values features scattering, we filtered the dataset by removing the outliers and considered only the values between the 25th and 75th percentiles (Fig. 7a-b). As a result, the number of grid nodes used to characterise distributed seismicity is 359
240 (Fig. 7c).

Figure 8 shows the variability of the *b*-values at different depths beneath the Etna region. Variations are noteworthy in the first 7 km of the crust, with low *b*-values (≤0.8) characterising the northern sector of the volcano around PF at very shallow levels of -2/-1 km, and higher *b*-values (≥1.2) in the central sector of Etna at a depth of 4 km, as in part highlighted by Murru et al. (1999).

245 Note that in the eastern sector including the SZ Timpe at depths ranging from 2 to 6 km bsl, the *b*-value pattern varies widely both in number (0.7-1.2) and in space (patches extending a few kilometres). Finally, a relatively minor variation of *b*-values (0.9-1.1) is evident at intermediate crustal levels in the range of 10-16 km, while at depths higher than 20 km low *b*-values (≤0.9) prevail again. This overall picture is consistent with the inter-event time distributions of earthquakes (Sicali et al., 2014), showing that features of earthquake occurrence in the western flank-central sector are very different from PF as well
250 as SZ Timpe, the latter more related with regional tectonics.

5 Individual sources: seismic rates from geometric-kinematic fault parameters

In the previous chapters seismic rates assigned to faults and area sources have been defined by historical-macroseismic and instrumental earthquake data. Taking advantage from the huge amount of geological field data and active tectonics evidence, we also performed a fault source modelling based on a purely geological approach: it converts the geometric-kinematic parameters representative of fault activity into a budget of seismic moment potentially released by the structure through a computational scheme that also accounts for a magnitude-size scaling relationship. In this way we obtain, for each fault, the most probable value of expected characteristic magnitude (M_{char}) with the associated standard deviation σ, the corresponding mean recurrence time (T_{mean}) and the aperiodicity factor α, that are the basic ingredients to compute earthquake occurrence probabilities, both under a Poissonian assumption as well as in a time-dependent perspective.

5.1 Method and input data

The analysis has been carried out through the software *FiSH*, a Matlab® routine developed to quantify the seismic activity of a fault from its geometric-kinematic parameters (Pace et al., 2015). The adopted approach is an evolution of the one by Peruzza et al. (2010) based on the criterion of 'segment seismic moment conservation' (Field et al., 1999). It takes into account the formal propagation of uncertainties in magnitude and slip-rate and uses directly the 3D fault geometry (length, dip-angle, thickness of the seismogenic layer) and slip-rate of a seismogenic structure. If a fault has a list of events associated to it, the mean values (magnitude, recurrence time) and their variability derive directly from historical or paleoseismological observations. However, the cases of effective repetition of major earthquakes on the same fault segment are definitely few in Italy, mostly along the Apennines in Central Italy (Galli et al., 2010; Cinti et al., 2011; Moro et al., 2013; Peruzza et al., 2011). At Mt Etna, some ten major earthquakes (M_L 4.3-5.2) repeatedly occurred along the fault segments of the Timpe and Pernicana systems (Azzaro et al., 2012b).

The *FiSH* code uses different empirical and analytical relationships available in the literature between fault geometry and the characteristics of the expected earthquake, in order to quantify several values of M_{max} and associated T_{mean}. Taking uncertainties of magnitude and slip-rate into account, the software provides budgeting of the seismic moment-rate. Finally, it uses the selected values to calculate the hazard rates, for a given exposure time, according to a Poissonian distribution or, in a time-dependent perspective that considers also the time elapsed since the last event, using some other widely used probability density function. For this study, the Brownian Passage Time (BPT, Matthews et al., 2002) is adopted to represent time-dependency.

Regarding our input data, the geometry, slip-rate and kinematics of the fault segments are constrained by detailed geological/geomorphological field investigations (Azzaro et al., 2012a) and geodetic data, the latter providing information on the vertical extension of faults as well as short-term slip-rates (Azzaro et al., 2013a). The 3D model of the individual sources considered in our application is shown in Fig. 9, together with the related geometric-kinematic parameters.

5.2 Magnitude-size scaling relationship for volcano-tectonic events

The characterization of an earthquake scaling relationship suitable for a volcanic domain such as Etna is a key step for modelling the rupture extent of these low to moderate magnitude events. Whereas empirical relationships derived for tectonic domains are largely available in the literature both for worldwide applications and regional contexts, those calibrated for active volcanic areas are relatively few. Stirling et al. (2013) mentioned among them those developed for thin crust volcano-tectonic contexts (Mason, 1996; Wesnousky, 2008), and the one specifically derived for the Taupo volcanic zone in New Zealand (Villamor et al., 2001).

At Mt Etna major shallow volcano-tectonic earthquakes produce surface faulting with end-to-end rupture lengths up to 6.5 km and vertical offsets up to 90 cm. Systematic historical investigations and recent observations have permitted the compilation of an earthquake rupture catalogue reporting some fifty coseismic faulting events (Azzaro, 1999, 2004). In the present analysis we use the most reliable observations of this dataset (43 data points) to derive a magnitude-scaling relationship specific for the Etna region, calibrated in the range M_W 2.8-5.2 (Fig. 10a).

In Fig. 10b, Mt. Etna relationship is plotted together with the ones available for tectonic and volcanic domains. Considering the approximations due to the use of different dimensional measurements – magnitude scales, rupture length vs. rupture area – and the limitation in extrapolating the fitting outside the original magnitude ranges, the comparison is fairly explanatory. We note analogies with respect to the relationship suggested by Villamor et al. (2001) for the Taupo volcanic zone, whereas discrepancies are substantial for thin crust volcano-tectonic context relationships proposed by Mason (1996) and Wesnousky (2008). Also the set of worldwide relationships by Wells and Coppersmith (1994) based on rupture length (RLD, SRL) tends, at different degrees, to overestimate the earthquake magnitude.

These considerations suggested to consider only the Etna and Taupo relationships for calculating the seismic rates of individual sources.

5.3 Maximum expected magnitude and related mean recurrence times

The *FiSH* code calculates the value of magnitudes expected for the full rupture of each fault by the above defined empirical scaling relationships. In order to check the geometrical consistency of the sources, it also estimates a maximum magnitude (M_{max}) according to: i) the scalar seismic moment (M_{Mo}), by using the modified formulation of magnitude (IASPEI, 2005) and a constant strain drop value of $3x10^{-5}$; ii) an additional constraint based on the aspect ratio relationships (M_{AR}) derived by Peruzza and Pace (2002). Fig. 11 shows probability curves of all the M_{max} values so far derived, assuming that a normal distribution represents the associated uncertainty, with a symmetrical bell-shape distributed around the central value; the maximum historical observed magnitude (M_{obs}) is also reported using the standard deviation of M assigned in the earthquake catalogue. The dashed curve (SUM) represents the summation of the probability density functions, whereas the vertical black line indicates the central value of its Gaussian fit to be considered as the reference mean value (M_{max}), with the associated standard deviation (σM_{max}) given by the horizontal dashed line (for details see Pace et al., 2015).

In general, the magnitude values calculated by the different relationships are not drastically different from each other if the wide uncertainty ranges are taken into account. Note that the M_{max} values are consistent with the M_{obs} for the simplest and best documented sources (FF, STF); in the cases of more complex structures (e.g. PF and SLF) that are characterised by coseismic slip and creeping alternating in space and even in time along strike (Azzaro, 2004), the maximum observed magnitude always lies in the range of full rupture magnitude minus one standard deviation ((M_{max}- σM_{max}).

Finally, the mean recurrence times (T_{mean}) associated to M_{max} values are computed accounting for slip rate uncertainties (see Fig. 9); they vary from 22 to 166 years (Tab. 2), periods generally consistent with those historically observed for the individual faults (see Tab 1). However, it should be stressed that T_{mean} is strongly dependent on the slip-rate values assigned to the faults (Fig. 9).

6 Conclusive remarks

We faced in this paper the problem of characterizing low magnitude, shallow seismic sources, capable of affecting the seismic hazard for short exposure times at Mt Etna, the largest active volcano in Europe. Usually the problem of ground shaking due to local superficial volcano-tectonic faults is discarded in favour of estimates based on large-scale regional crustal faults capable of generating strong earthquakes (M>6); in addition, other major threats related to the eruptive activity, or to the flank instability (Acocella et al., 2013; Acocella and Puglisi, 2013), can be first-order priorities for land planning and risk mitigation actions. But on Mt Etna slopes, several inhabited localities have been repeatedly and heavily damaged as a consequence of local earthquakes with M<5.5 that may be connected to the eruption phases or not. In the documented history, such damage occurred on average every 20-25 years, the last sequence along the S. Venerina fault (SVF) in 2002. To tackle these issues, the Italian Department of Civil Defense (DPC) funded in the last decade two research programs on Mt Etna aimed at mitigating, among others, the seismic risk (Acocella and Puglisi, 2010; Azzaro and De Rosa, 2016). In this framework we started to characterise, with different methodological approaches, shallow sources and finally to assess the seismic hazard at the local scale of the volcano (Azzaro et al., 2012b, 2013b, 2016; Peruzza et al., 2017). Some basic ideas have driven our analyses i) a few years of a high quality seismic monitoring in an 'interseismic' period can be representative of the long-term seismic rates of faults: ii) fault size and slip rate can constrain the maximum magnitude and the seismic moment budgeting, and geologic-geodetic derived seismic rates must be coherent with historical and instrumental data. If such ideas are true, we can extend the modelling of seismic sources to the whole volcanic complex by addressing 'unknown' faults by distributed point sources, and we are no longer forced to use independent events (i.e. the declustered earthquake catalogue, assuring stationarity of the process), but we can compute the probabilities of events for any magnitude-frequency distribution for a generalized non-Poisson model.

We focussed our analyses on two main volcano-tectonic fault systems evaluated at the surface and by geophysical investigations. Table 2 reports an overview of the relevant parameters to be used as input data in the companion paper by Peruzza et al. (2017). The Pernicana fault (PF) is an E-W oriented, S-dipping system of brittle and creeping transtensional

segments: very shallow instrumental seismicity (located very often above the sea level) depicts quite well the 3D geometry of this structure characterized by low b-values (<0.7). The Timpe system in the SE flank is a group of nearly vertical normal faults. Their deep geometry cannot be precisely detected even by the high-quality instrumental earthquake dataset available in the last years. Area seismic sources have been depicted with increasing level of detail by using space buffers around the surface trace faults. Taken as a whole, the FMD of the SZ Timpe - as derived from the instrumental dataset of 2005-2015, a period that represents the 'interseismic background' level not affected by main earthquake sequences - is similar to the FMDs and depth distributions of the Moscarello (MF) and S. Leonardello faults (SLF), whilst the Fiandaca fault (FF), S. Tecla (STF) and S. Venerina faults (SVF) show, respectively, lower and higher b-values and activity rates.

Regarding the seismicity rates to be assigned to the faults, we note a global consistency by using the geometric-kinematic approach, and by using the historical earthquake dataset. The maximum magnitudes (M_{max}) calculated by scaling relationships appear ca. 0.3-0.6 units higher than the observed magnitudes (M_{obs}), whilst the related mean recurrence times (T_{mean}) are sometimes lower, modulated by the fast slip rates. A number of reasons may account for these discrepancies, such as: i) uncertainties of the geologic slip-rate estimations; ii) geometries of the modelled faults are not well constrained; iii) difficulty in discriminating pre- and post-seismic slip with respect the coseismic rupture length; iv) the role of fault segments in accommodating deformation (slip-rate partitioning).

Finally, the aperiodicity coefficients suggest sensitivity tests and care in modelling faults by a time-dependent approach: the α's obtained by geologic data indicate a quasi-stationary behaviour of the maximum-sized events, whilst the one calculated from the intertimes of historical earthquakes suggests a certain degree of periodicity. Both the seismicity rates for M_{max}, however, are within the uncertainties of rates derived by the GR relationships of instrumental data.

This work represents the effort to provide the international scientific community with original procedures and methodological approaches to produce hazards maps in other volcanic areas, and improves basic knowledge of seismogenic processes at Etna.

Acknowledgements

This study has benefited from funding provided by the Italian Presidenza del Consiglio dei Ministri –Dipartimento della Protezione Civile (DPC), in the frame of the 2012-14 Agreement with Istituto Nazionale di Geofisica e Vulcanologia-INGV, Project V3 "Multi-disciplinary analysis of the relationships between tectonic structures and volcanic activity".

This paper does not necessarily represent DPC official opinion and policies. The authors are grateful to R. Gee for having provided a revision of the English text.

References

375   Acocella, V., Puglisi, G. and Amelung, F.: Flank instability, eruptions, seismicity and hazard: the case of Mt. Etna, J. Volcanol. Geoth. Res., 251, 1-4, 2013.

Acocella, V. and Puglisi, G.: How to cope with volcano flank dynamics? A conceptual model behind possible scenarios for Mt. Etna, J. Volcanol. Geoth. Res., 251, 137-148, 2013.

Acocella, V. and Puglisi, G.: Hazard mitigation of unstable volcanic edifices, Eos, 91, 40, 357-358, 2010.

380   Alparone, S., Barberi, G., Bonforte, A., Maiolino, V. and Ursino, A.: Evidence of multiple strain fields beneath the eastern flank of Mt. Etna volcano (Sicily, Italy) deduced from seismic and geodetic data during 2003–2004, Bull. Vulcanol., 73, 869-885, 2011.

Alparone, S., Barberi, G., Cocina, O., Giampiccolo, E., Musumeci, C. and Patanè, D.: Intrusive mechanism of the 2008–2009 Mt. Etna eruption: constraints by tomographic images and stress tensor analysis, J. Volcanol. Geoth. Res., 229-230, 50-
385   63, doi: 10.1016/j.jvolgeores.2012.04.001, 2012.

Alparone, S., Maiolino, V., Mostaccio, A., Scaltrito, A., Ursino, A., Barberi, G., D'Amico, S., Di Grazia, G., Giampiccolo, E., Musumeci, C., Scarfì, L. and Zuccarello, L.: Instrumental seismic catalogue of Mt. Etna earthquakes (Sicily, Italy): ten years (2000-2010) of instrumental recordings, Annals of Geophysics, 58, S0435, doi: 10.4401/ag-6591, 2015.

Azzaro, R: Earthquake surface faulting at Mount Etna volcano (Sicily) and implications for active tectonics, J. Geodyn., 28,
390   193-213, 1999.

Azzaro, R.: Seismicity and active tectonics in the Etna region: constraints for a seismotectonic model. In: Bonaccorso A., Calvari S., Coltelli M., Del Negro C. and Falsaperla S. (eds), Mt. Etna: Volcano laboratory, American Geophysical Union, 205-220, doi:10.1029/GM143, 2004.

Azzaro, R., Barbano, M.S., Antichi, B. and Rigano, R.: Macroseismic catalogue of Mt. Etna earthquakes from 1832 to 1998.
395   Upgrade 1999-2008, Acta Volcanologica, 12 (1), 3-36, 2000.

Azzaro, R., Bonforte, A., Branca, S. and Guglielmino, F.: Geometry and kinematics of the fault systems controlling the unstable flank of Etna volcano (Sicily), J. Volcanol. Geoth. Res., 251, 5-15, 2013a.

Azzaro, R., Branca, S., Gwinner, K. and Coltelli, M.: The volcano-tectonic map of Etna volcano, 1:100.000 scale: an integrated approach based on a morphotectonic analysis from high-resolution DEM constrained by geologic, active faulting
400   and seismotectonic data, Italian Journal of Geosciences, 131, 153-170, 2012a.

Azzaro, R. and Castelli, V.: Materials for a catalogue of Mt. Etna earthquakes from 1600 to 1831, Quaderni di Geofisica, 123, 278 pp., ISSN 1590-2595, 2015.

Azzaro, R., D'Amico, S. and Tuvè, T.: Estimating the magnitude of historical earthquakes from macroseismic intensity data: new relationships for the volcanic region of Mount Etna (Italy), Seism. Res. Lett. 82, 4, 533-544, 2011.

405   Azzaro, R., D'Amico, S. and Tuvè, T.: Seismic hazard assessment in the volcanic region of Mt. Etna (Italy): a probabilistic approach based on macroseismic data applied to volcano-tectonic seismicity, Bull. Earth. Eng., 17 (7), 1813-1825, 2016.

Azzaro, R., D'Amico, S., Peruzza, L. and Tuvè, T.: Earthquakes and faults at Mt. Etna (Southern Italy): problems and perspectives for a time-dependent probabilistic seismic hazard assessment in a volcanic region, Boll. Geofis. Teor. App., 53, 75-88, 2012b.

410   Azzaro, R., D'Amico, S., Peruzza, L. and Tuvè, T.: Probabilistic seismic hazard at Mt. Etna (Italy): the contribution of local fault activity in mid-term assessment, J. Volcanol. Geoth. Res., 251, 158-169, 2013b.

Azzaro, R. and De Rosa, R.: Project V3, multi-disciplinary analysis of the relationships between tectonic structures and volcanic activity (Etna, Vulcano-Lipari system), Final Report November 1st, 2014 – June 30th, 2015, Agreement INGV-DPC 2012-2021, Volcanological programme 2012-2015, Miscellanea INGV, 29, 172 pp., ISSN 2039-6651 , 2016a.

415   Azzaro, R. and De Rosa, R.: Understanding volcanic eruptions where plates meet, Eos, 97, doi:10.1029/2016EO052359, 2016b.

Bonforte, A., Guglielmino, F., Coltelli, M., Ferretti, A. and Puglisi, G.: Structural assessment of Mount Etna volcano from Permanent Scatterers analysis, Geochemistry Geophysics Geosystems, 12, Q02002, doi: 10.1029/2010GC003213, 2011.

Bousquet, J.C. and Lanzafame, G.: The tectonics and geodynamics of Mt. Etna: synthesis and interpretation of geological
420   and geophysical data. In: Bonaccorso A., Calvari S., Coltelli M., Del Negro C. and Falsaperla S. (eds), Mt. Etna: Volcano laboratory, American Geophysical Union, Geophysical monograph, 143, pp. 29-47, doi:10.1029/GM143, 2004.

Bozzano, F., Gaeta, M., Lenti, L., Martino, S., Paciello, A., Palladino, D.M. and Sottili, G.: Modeling the effects of eruptive and seismic activities on flank instability at Mount Etna, Italy, J. Geophys. Res. Solid Earth, 118, doi:10.1002/jgrb.50377, 2013.

425   Bruno, V., Mattia, M., Aloisi, M., Palano, M., Cannavò, F. and Holt, W.E.: Ground deformations and volcanic processes as imaged by CGPS data at Mt. Etna (Italy) between 2003 and 2008, J. Geophys. Res., 117, B07208, doi:10.1029/2011JB009114, 2012.

Cinti, F.R., Pantosti, D., De Martini, P.M., Pucci S., Civico, R., Pierdominici, S., Cucci, L., Brunori, C.A., Pinzi, S. and Patera, A.: Evidence for surface faulting events along the Paganica fault prior to the 6 April 2009 L'Aquila earthquake
430   (central Italy), J. Geoph. Res., 116, B07308, doi:10.1029/2010JB007988, 2011.

CMTE Working Group: Catalogo Macrosismico dei Terremoti Etnei dal 1600 al 2013. INGV, Catania, http://www.ct.ingv.it/macro/etna/html_index.php, 2017.

Cocina, O., Alparone, S., Barberi, G., Giampiccolo, E., Maiolino, V., Musumeci, C., Saraò, A., Scarfì, L. and Ursino, A.: Space-time distribution of seismicity and strain release, also in relation with the main recharging phases of the volcano. In:
435   Azzaro, R., De Rosa, R., Project V3: multi-disciplinary analysis of the relationships between tectonic structures and volcanic activity (Etna, Vulcano-Lipari system), Final Report, Miscellanea INGV, 29, pp. 44-49, ISSN 2039-6651, https://sites.google.com/a/ingv.it/volcpro2014/, 2016.

De Guidi, G., Barberi, G., Barreca, G., Bruno, V., Cultrera, F., Grassi, S., Imposa, S., Mattia, M., Monaco, C., Scarfì, L. and Scudero, S.: Geological, seismological and geodetic evidence of active thrusting and folding south of Mt. Etna (eastern
440   Sicily): revaluation of "seismic efficiency" of the Sicilian Basal Thrust, J. Geodyn., 90, 32–41, 2015.

De Guidi, G., Scudero, S. and Gresta, S.: New insights into the local crust structure of Mt. Etna volcano from seismological and morphotectonic data, J. Volcanol. Geoth. Res., 223-224, 83-92, 2012.

Field, E.H., Johnson, D.D. and Dolan, J.F.: A mutually consistent seismic-hazard source model for Southern California, Bull. Seism. Soc. Am., 89, 559-578, 1999.

445   Galli, P., Giaccio, B. and Messina, P.: The 2009 central Italy earthquake seen through 0.5 Myr- long tectonic history of the L'Aquila faults system, Quat. Sci. Rev., 29, 3768–3789, 2010.

Gasperini, P., Gresta, G. and Mulargia, F.: Statistical analysis of seismic and eruptive activities at Mt. Etna during 1978-1987, J. Volcanol. Geoth. Res., 40, 317-325, 1990.

Gresta, G., Marzocchi, W. and Mulargia, F.: Is there a correlation between larger local earthquakes and the end of eruptions
450   at Mount Etna volcano, Sicily? Geophys. J. Int., 116, 230-232, 1994.

Grünthal, G. (Ed.): European Macroseismic Scale 1998 (EMS-98), European Seismological Commission, Subcommission on Engineering Seismology, Working Group Macroseismic Scale, 15, Luxembourg, pp. 99, http://www.ecgs.lu/cahiers-bleus/, 1998.

Gruppo Analisi Dati Sismici: Catalogo dei terremoti della Sicilia Orientale - Calabria Meridionale (1999-2015). INGV,
455   Catania, http://www.ct.ingv.it/ufs/analisti/, 2016.

International Association of Seismology and Physics of the Earth's Interior (IASPEI): Summary of Magnitude Working Group recommendations on standard procedures for determining earthquake magnitudes from digital data, 2013, ftp://ftp.iaspei.org/pub/commissions/CSOI/Summary_WG_recommendations_20130327.pdf (last accessed March 2017).

Kanamori, H.: The energy release in great earthquakes, J. Geophys. Res., 82, 2981-2987, 1977.

460   Lavecchia, G., Ferrarini, F., De Nardis, R., Visini, F. and Barbano, M.S.: Active thrusting as a possible seismogenic source in Sicily (Southern Italy): Some insights from integrated structural-kinematic and seismological data, Tectonophysics, 445, 145–167, 2007.

Mason, D.B.: Earthquake magnitude potential of the intermountain seismic belt, USA, from surface-parameter scaling of late Quaternary faults, Bull. Seismol. Soc. Am., 86, 1487–1506, 1996.

465   Matthews, M.V., Ellsworth, W.L. and Reasenberg, P.A.: A Brownian model for recurrent earthquakes, Bull. Seism. Soc. Am., 92, 2233-2250, 2002.

Meletti, C., Galadini, F., Valensise, G., Stucchi, M., Basili, R., Barba, S., Vannucci, G. and Boschi, E.: A seismic source zone model for the seismic hazard assessment of the Italian territory, Tectonophysics., 450, 85-108, 2008.

Moro, M., Gori, S., Falcucci, E., Saroli, M., Galadini, F. and Salvi, S.: Historical earthquakes and variable kinematic
470   behaviour of the 2009 L'Aquila seismic event (central Italy), causative fault, revealed by paleoseismological investigations, Tectonoph., 583, 131-144, 2013.

Mostaccio, A., Tuvè, T., Patanè, D., Barberi, G. and Zuccarello, L.: Improving seismic surveillance at Mt. Etna volcano by probabilistic earthquake location in a 3D model, Bull. Seism. Soc. Am., 103, 4, 2447-2459, 2013.

Murru, M., Montuori, C., Wyss, M. and Privitera, E.: The locations of magma chambers at Mt. Etna, Italy, mapped by *b*-values, Geophys. Res. Lett., 26, 10, 2553-2556, 1999.

Nercessian, A., Hirn, A. and Sapin, M.: A correlation between earthquakes and eruptive phases at Mt. Etna: an example and past occurrences, Geophys. J. Int., 105, 131-138, 1991.

Pace, B., Visini, F. and Peruzza, L.: FiSH: MATLAB tools to turn fault data into seismic hazard models, Seism. Res. Lett., 87, 2a, doi: 10.1785/0220150189, 2016.

Palano, M.: Episodic slow slip events and seaward flank motion at Mt. Etna volcano (Italy), J. Volcanol. Geoth. Res., 324, 8–14, 2016.

Parsons, T.: Monte Carlo method for determining earthquake recurrence parameters from short paleoseismic catalogs: example calculations for California, J. Geophys. Res., 113, B03302, 2008, doi:10.1029/2007JB004998

Patanè, D., Cocina, O., Falsaperla, S., Privitera, E. and Spampinato, S.: Mt. Etna volcano: a seismological framework. In: Calvari, S., Bonaccorso, A., Coltelli, M., Del Negro, C., Falsaperla, S. (Eds.), Mt. Etna: Volcano Laboratory, Am. Geophys. Union, Geophys. Monogr., vol. 143, pp. 147–165, 2004.

Peruzza, L. (coord.): Project S2 Final Scientific Report Agreement INGV-DPC 2012-2021, Seismological Program 2012-13, https://sites.google.com/site/ingvdpc2012progettos2/documents/, 2013.

Peruzza, L. and Pace, B.: Sensitivity analysis for seismic source characteristics to probabilistic seismic hazard assessment in Central Apennines (Abruzzo area), Boll. Geofis. Teor. App., 43, 79-100, 2002.

Peruzza, L., Pace, B. and Cavallini, F.: Error propagation in time-dependent probability of occurrence for characteristic earthquakes in Italy, J. Seism., 14, 119-141, 2010.

Peruzza, L., Pace, B. and Visini, F.: Fault-based earthquake rupture forecast in Central Italy: remarks after the L'Aquila Mw 6.3 event. Bull. Seism. Soc. Am., 101, 404-412, 2011.

Peruzza, L., Azzaro, R., Gee, R., D'Amico, S., Langer, H., Lombardo, G., Pace, B., Pagani, M., Panzera, F., Ordaz, M., Suarez, M.L. and Tusa, G.: When probabilistic seismic hazard climbs volcanoes: the Mt Etna case, Italy. Part II: computational implementation and first results, Submitted to NHESS, Special Issue (this volume), 2017.

Rasà, R., Azzaro, R. and Leonardi, O.: Aseismic creep on faults and flank instability at Mount Etna volcano, Sicily, in: McGuire, W.J., Jones, A.P., Neuberg J. (Eds.), Volcano instability on the Earth and other planets, Geological Society of London, Special Publications, 110, 179-192, 1996.

Saraò, A., Cocina, O., Moratto, L. and Scarfì, L.: Earthquake features through the seismic moment tensor. In: Azzaro, R., De Rosa, R., Project V3: multi-disciplinary analysis of the relationships between tectonic structures and volcanic activity (Etna, Vulcano-Lipari system), Final Report, Miscellanea INGV, 29, pp. 98-101, ISSN 2039-6651, https://sites.google.com/a/ingv.it/volcpro2014/, 2016.

Sicali, S., Barbano, M.S., D'Amico, S. and Azzaro R.: Characterization of seismicity at Mt. Etna volcano (Italy) by inter-event time distribution, J. Volcanol. Geotherm. Res., 270, 1-9, 2014.

Solaro, G., Acocella, V., Pepe, S., Ruch, J., Neri, M. and Sansosti, E.: Anatomy of an unstable volcano from InSAR: multiple processes affecting flank instability at Mt. Etna, 1994–2008, J. Geophys. Res., 115, B10405, 2010.

Schwartz, D.P. and Coppersmith, K.J.: Fault behaviour and characteristic earthquake: examples from the Wasatch and San Andreas fault zones, J. Geoph. Res., 89 (B7), 5681-5698, 1984.

Stirling, M., Godet, T., Berryman, K. and Litchfield, N.: Selection of earthquake scaling relationships for seismic-hazard analysis, Bull. Seism. Soc. Am., 103, 2993-3011, 2013.

Scarfì, L., Barberi, G., Musumeci, C. and Patanè, D.: Seismotectonics of northeastern Sicily and southern Calabria (Italy): new constraints on the tectonic structures featuring in a crucial sector for the central Mediterranean geodynamics, Tectonics, 35, 812–830, doi:10.1002/2015TC004022, 2016.

Stucchi, M., Meletti, C., Montaldo, V., Crowley, H., Calvi, G.M. and Boschi, E.: Seismic Hazard Assessment (2003-2009) for the Italian Building Code, Bull. Seism. Soc. Am., 101 (4), 1885-1911, 2011.

Traversa, P. and Grasso, J.R.: How is volcano seismicity different from tectonic seismicity?, Bull. Seism. Soc. Am., 100, 1755-1769, 2010.

Tuvè, T., D'Amico, S. and Giampiccolo, E.: A new M_D-M_L relationship for Mt. Etna earthquakes (Italy), Annals Geophysics, 58, S0657, 2015.

Villamor, P., Berryman, R.K.R., Webb, T., Stirling, M., McGinty, P., Downes, G., Harris, J. and Litchfield, N.: Waikato Seismic Loads: revision of Seismic Source Characterisation, GNS Client Report, 59, 2001.

Wells, D.L. and Coppersmith, K.J.: New empirical relationships among magnitude, rupture length, rupture area, and surface displacement, Bull. Seism. Soc. Am., 84, 974-1002, 1994.

Wesnousky, S.G.: Displacement and geometrical characteristics of earthquake surface ruptures: issues and implications for seismic-hazard analysis and the process of earthquake rupture, Bull. Seism. Soc. Am., 98, 1609-1632, 2008.

Wiemer, S.: A software package to analyze seismicity: ZMAP, Seism. Res. Lett., 72, 374-383, 2001.

Wiemer, S. and Wyss, M.: Mapping spatial variability of the frequency-magnitude distribution of earthquakes, Advances in Geophysics, 45, 259-302, 2002.

Woessner, J., Danciu, L., Giardini, D. Crowley, H., Cotton, F., Grünthal, G., Valensise, G., Arvidsson, R., Basili, R., Demircioglu, M.N., Hiemer, S., Meletti, C., Musson, R.W., Rovida, A.N., Sesetyan, K., Stucchi, M. and the SHARE consortium: The 2013 European Seismic Hazard Model: key components and results, Bull. Earthq. Eng., 2015, doi:10.1007/s10518-015-9795-1

Zhang H., Thurber C. and Bedrosian P.: Joint inversion for Vp, Vs, and Vp/Vs at SAFOD, Parkfield, California. Geochemistry Geophysics Geosystems. 10, Q110032, doi:10.1029/2009GC002709, 2009.

Zöller, G., Hainzl, S. and Holschneider, M.: Recurrent large earthquakes in a fault region: what can be inferred from small and intermediate events?, Bull. Seism. Soc. Am., 98 (6), 2641–2651, doi: 10.1785/0120080146, 2008.

540

	PF	MF-SLF	STF-SVF	FF
Effective depth (km)	0 to 2.0	0 to 5.0	0 to 5.0	0 to 2.0
b-value	0.64 ± 0.06	0.91 ± 0.08	1.13 ± 0.16	0.84 ± 0.15
annual *a*-value	2.08	2.51	2.73	1.72

Table 1: Effective depth, b and a coefficients of the GR relationship for each SZ, obtained from the instrumental earthquake dataset (2005-2015).

545

Fault	Geological-kinematic						Instrumental eqs dataset		Historical eqs dataset			
	T_{mean} (yr)	α	M_{max}	$σM_{max}$	M_0 rate (Nm)	μ (GPa)	α	M_{min}	M_{obs}	$σM_{obs}$	T_{mean} (yr)	α
Pernicana (PF)	28	1.04	5.0	0.3	1.42E+15	11	0.52	4.3	4.7	0.30		
Fiandaca (FF)	166	1.04	4.9	0.3	1.70E+14	12	0.62	4.3	4.6	0.36	71	
S. Tecla (STF)	53	1.08	5.3	0.3	2.12E+15	15	0.78	4.3	5.2	0.36	71	0.36*
S. Venerina (SVF)	45	1.05	5.0	0.3	8.85E+14	15	0.78	4.3	4.6	0.36	71	0.42
Moscarello (MF)	119	1.42	5.5	0.4	1.88E+15	15	0.66	4.3	4.9	0.36	71	
S. Leonardello (SLF)	22	1.37	4.8	0.4	9.06E+14	15	0.66	4.3	4.0	0.36	71	

Table 2: Comparison with estimations based on historical and instrumental earthquake datasets. Abbreviations: T_{mean}, mean recurrence time; α, aperiodicity factor; M_{max}, maximum magnitude obtained by the FiSH code and related standard deviation ($σM_{max}$); M_0, moment rate; μ, shear modulus; M_{min}, minimum magnitude for which is calculated the probability of occurrence (Mmax-sd Mmax, see Peruzza et al., 2017). Asterisk indicates the value obtained by the bootstrap analysis.

550
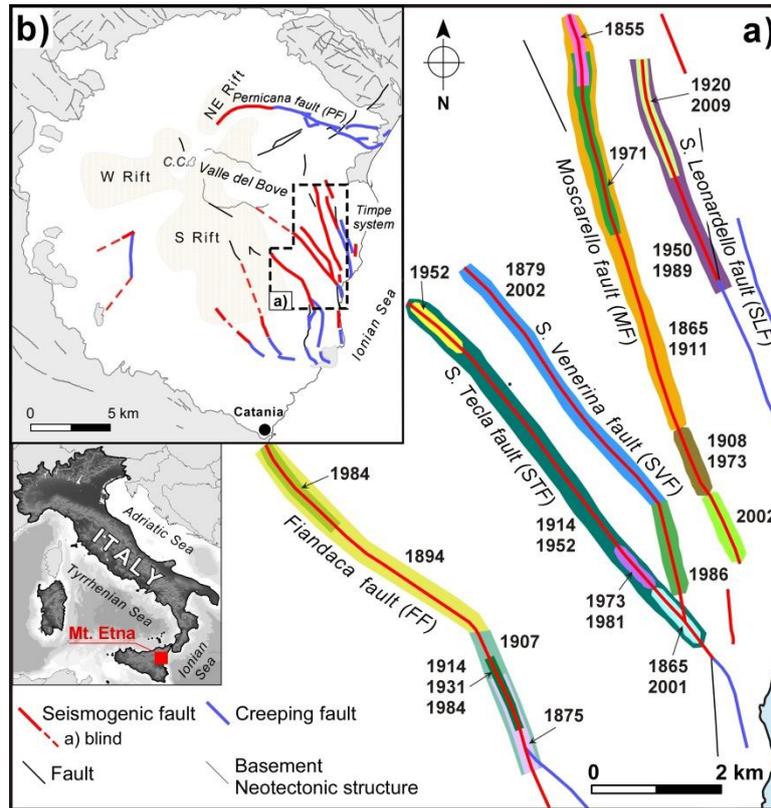
Figure 1: fault systems in the study area: a) Patterns of historical surface faulting along the southeastern flank of Mt Etna (Timpe tectonic system); colors represent coseismic ruptures related to different earthquakes (modified from Azzaro, 1999). b) Seismotectonic model of Etna (from Azzaro et al., 2012a). In beige the rift zones, i.e. high frequency of opening of eruptive fissures; in grey the sedimentary and metamorphic basement underlying the volcano.

555
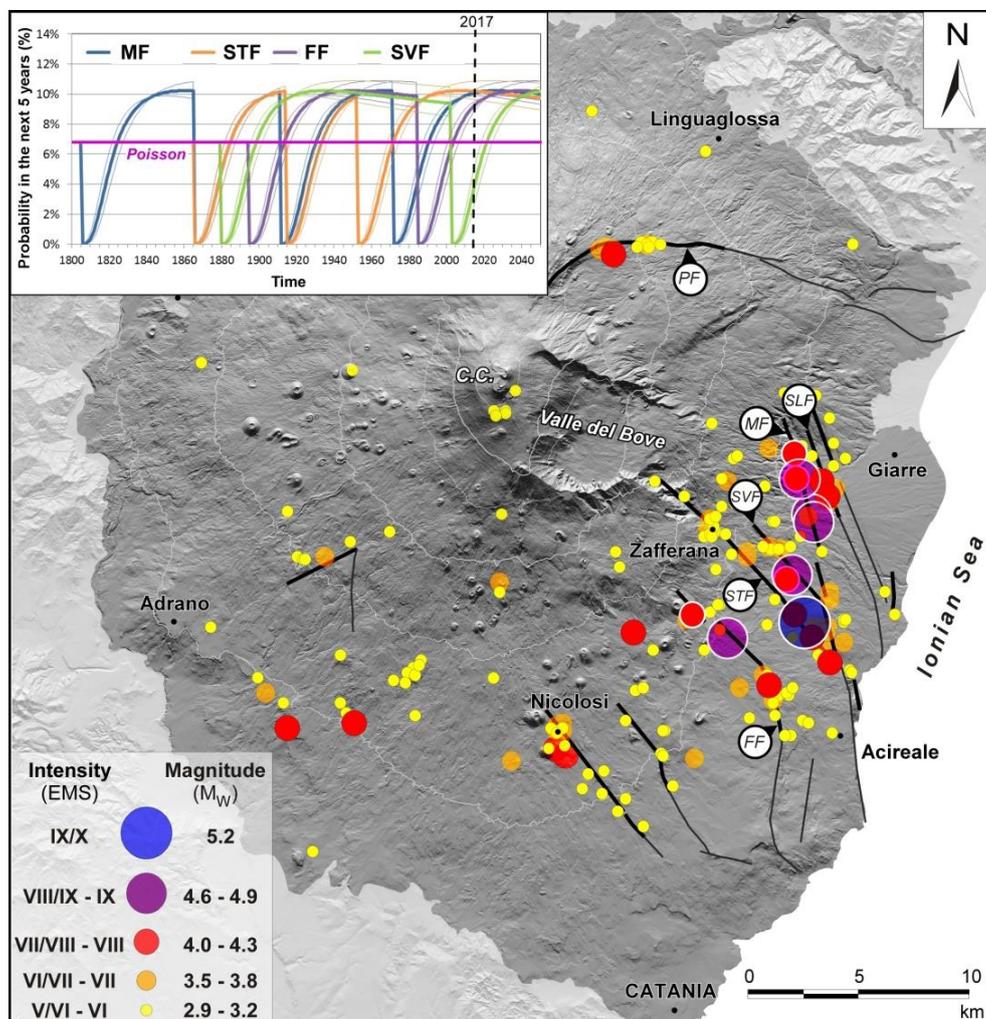
Figure 2: Distribution of the historical seismicity in the Etna region from 1600 to 2015 (data from CMTE Working Group, 2017). Major events considered for the analysis are marked in white; fault pattern and abbreviations as in Fig. 1, C.C. indicates the central craters. Inset map shows the retrospective test of the time-dependent model based on intertimes and *b*-values of faults: colored curves indicate the variation in time of the conditional probability assigned to the faults of the SZ Timpe, in the next 5 years. Before the first event assigned to each fault, the probability is assumed as Poissonian; following the earthquake, the probability curve collapses and progressively increases until the next rupture (from Azzaro et al., 2013b).
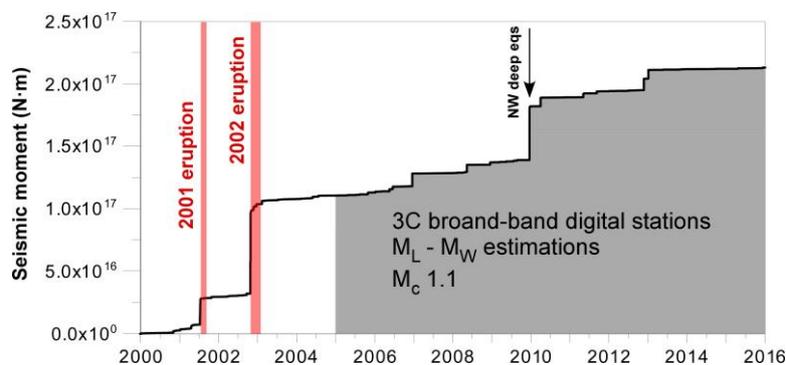
Figure 3: Cumulative seismic moment from 2000 to 2015 (calculated according to Kanamori, 1977). The periods marked in red indicate the main flank eruptions; in grey the time-span selected for the analysis. Note that the step in the seismic release at the end of 2009 is related with a seismic sequence occurred in the NW sector of Etna at a depth of 24-28 km, not affecting the characterization of shallow seismicity.

570
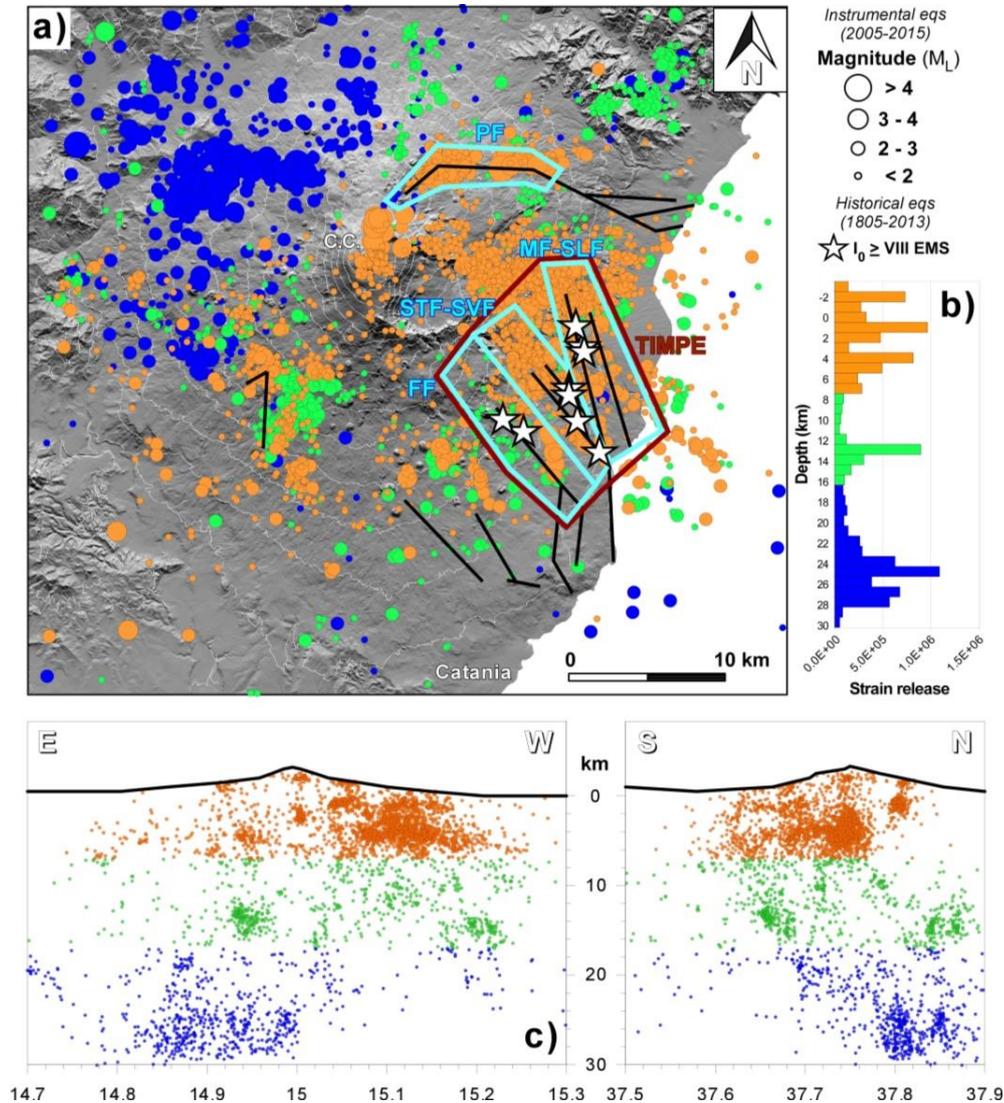
Figure 4: a) Historical and instrumental seismicity used for characterizing seismic sources at Etna. Areas in light blue indicate the
seismic zones: PF, Pernicana fault (295 eqs.); MF-SLF, Moscarello and S. Leonardello faults (354 eqs.); STF-SVF, S. Tecla and S.
Venerina faults (313 eqs.); FF, Fiandaca fault (69 eqs.); Timpe (919 eqs.). Solid black lines represent the simplified pattern of
active faults. **b)** Distributions of seismic strain release vs. focal depth for the 2005-2015 instrumental earthquake dataset referred
to the whole Etna region. **c)** Cross-sections of the 2005-2015 instrumental earthquakes beneath the volcano.
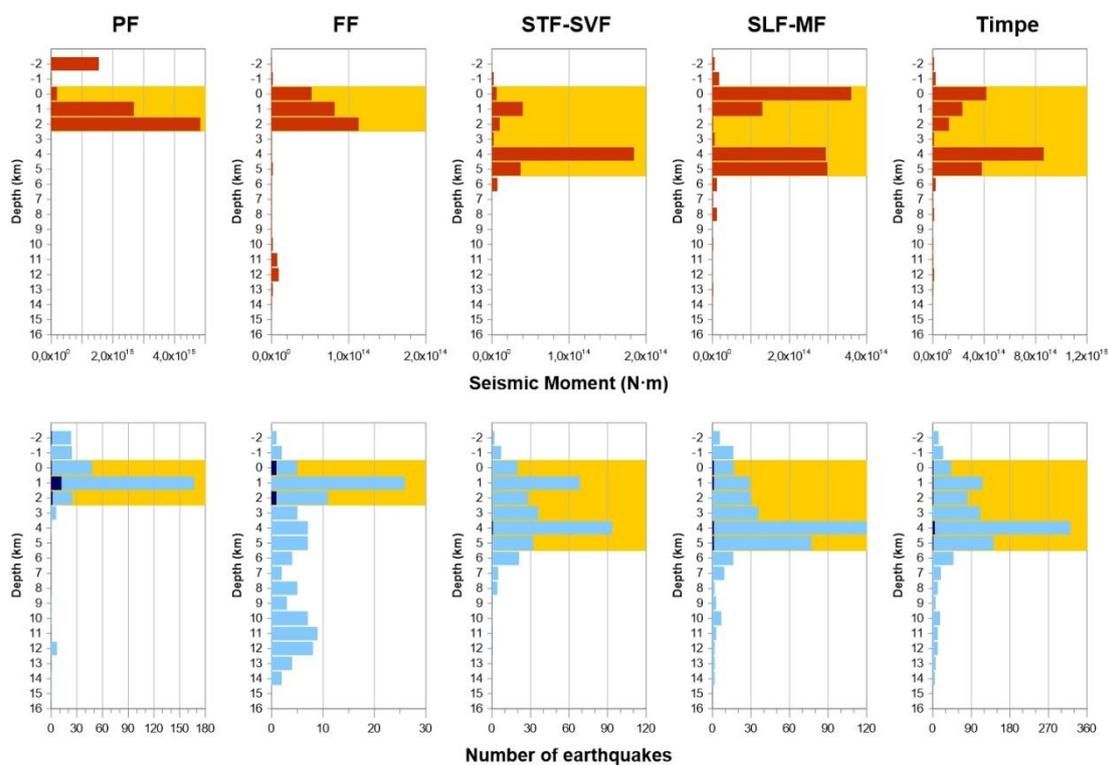
Figure 5: Distributions of seismic strain release (top) and number of earthquakes (bottom) vs. focal depth for the SZs considered in the model. Dark blue histograms indicate the number of earthquakes with $M_W \geq 3.0$. The effective depth is marked in orange. Abbreviations as in Fig. 4.

585

Instrumental dataset (2005-2015)   ◆ Macroseismic dataset (1832-2015)
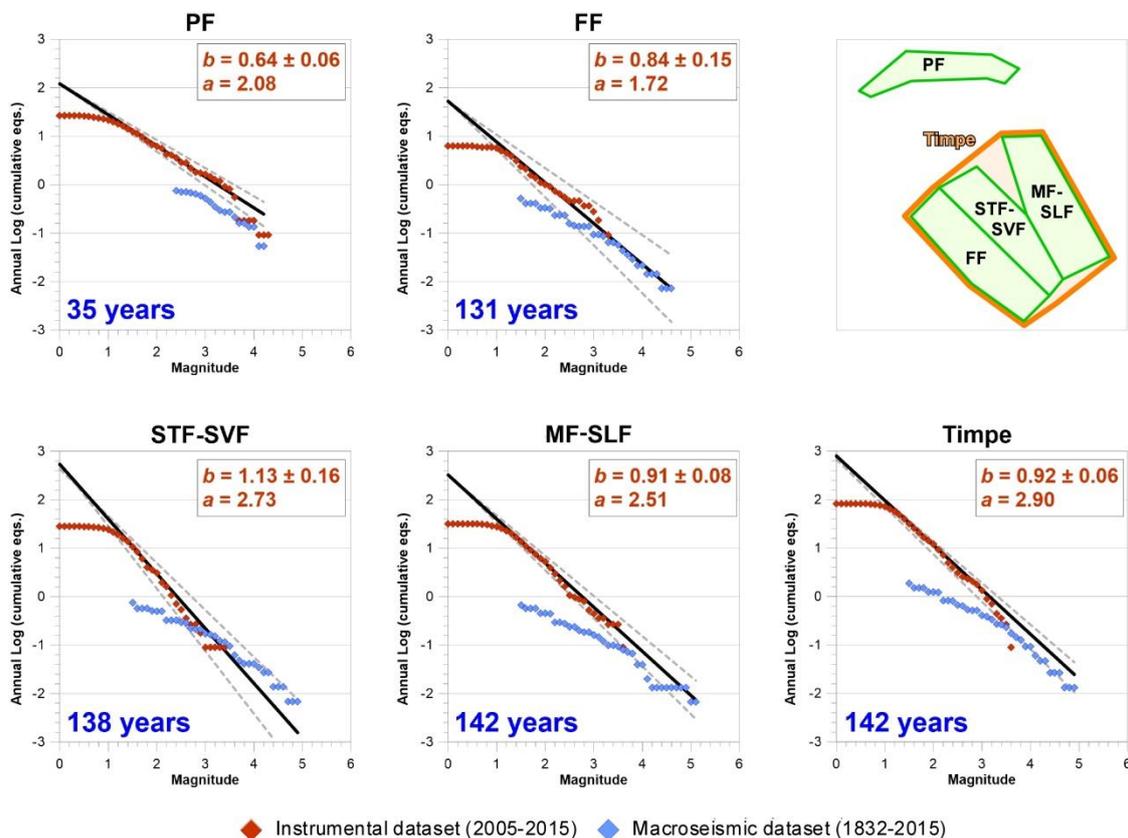
Figure 6: Frequency Magnitude Distribution for each SZ. Red dots refer to the instrumental dataset, blue dots to the macroseismic one; dotted lines indicate uncertainties with regards to the GR relationship (black line). *b*- and *a*-values are obtained from the instrumental earthquake dataset. Years indicate the time-window of the historical macroseismic catalogue. Data are normalized to one year. Abbreviations as in Fig. 4.

590
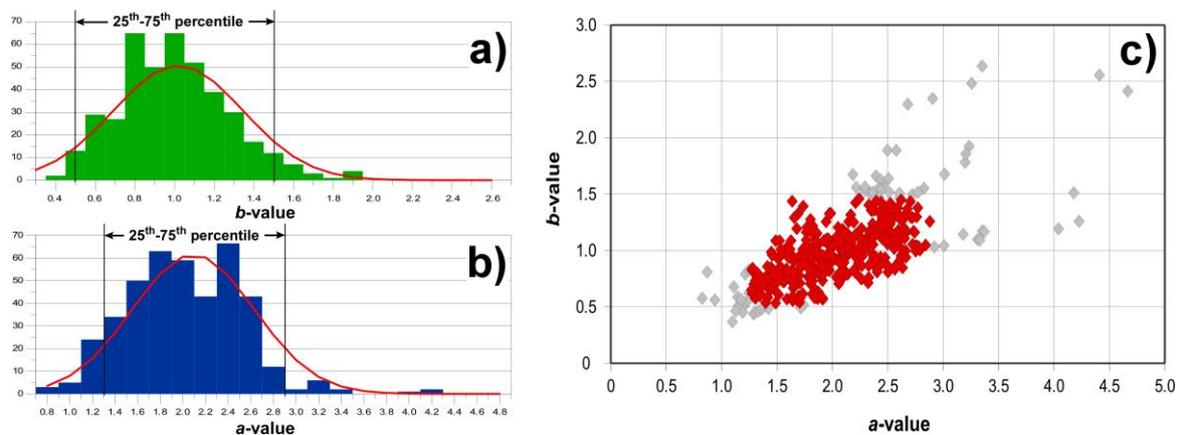
Figure 7: a-b) Histograms showing the frequency distribution of *b*- and *a*-values. c) Plot of *a*- and *b*-values obtained for the grid nodes; discarded values are in grey.
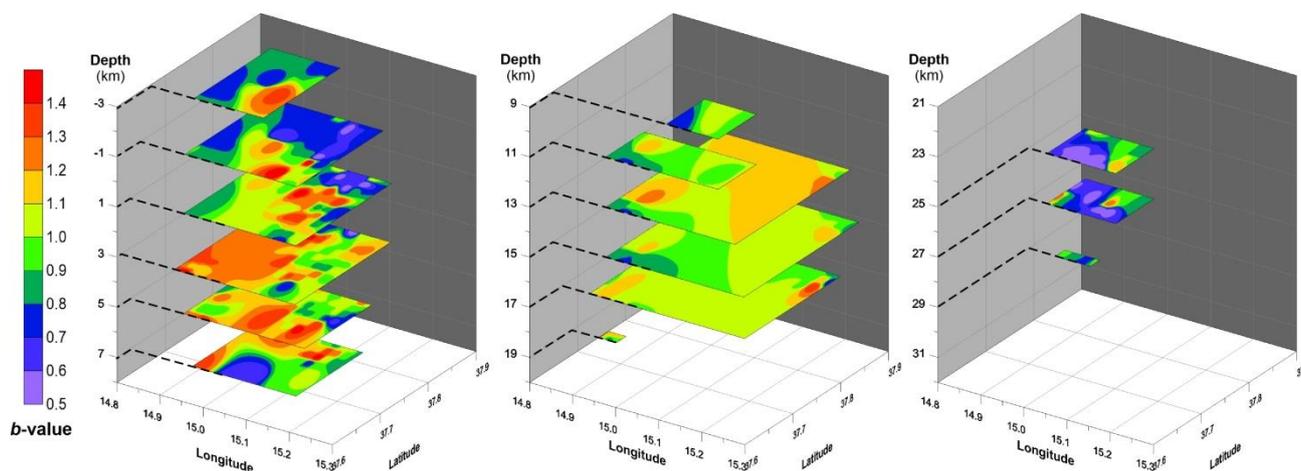
Figure 8: Distribution of the *b*-values beneath Etna calculated from the instrumental earthquake catalogue (2005-2015): the horizontal sections show the grids at different depths.

Fault	Id	Length (km)	Down-dip Heigth (km)	Dip (°)	Slip-rate max (mm/yr)	Slip-rate min (mm/yr)
Pernicana	PF	10.3	4.2	45	5.4	4.7
Fiandaca	FF	7.7	1.5	90	2.1	1.7
S. Tecla	STF	7.6	5.5	90	4.5	2.3
S. Venerina	SVF	5.6	5.5	90	2.1	1.7
Moscarello	MF	11.0	5.9	70	2.7	1.4
S. Leonardello	SLF	4.0	5.9	70	2.6	2.6
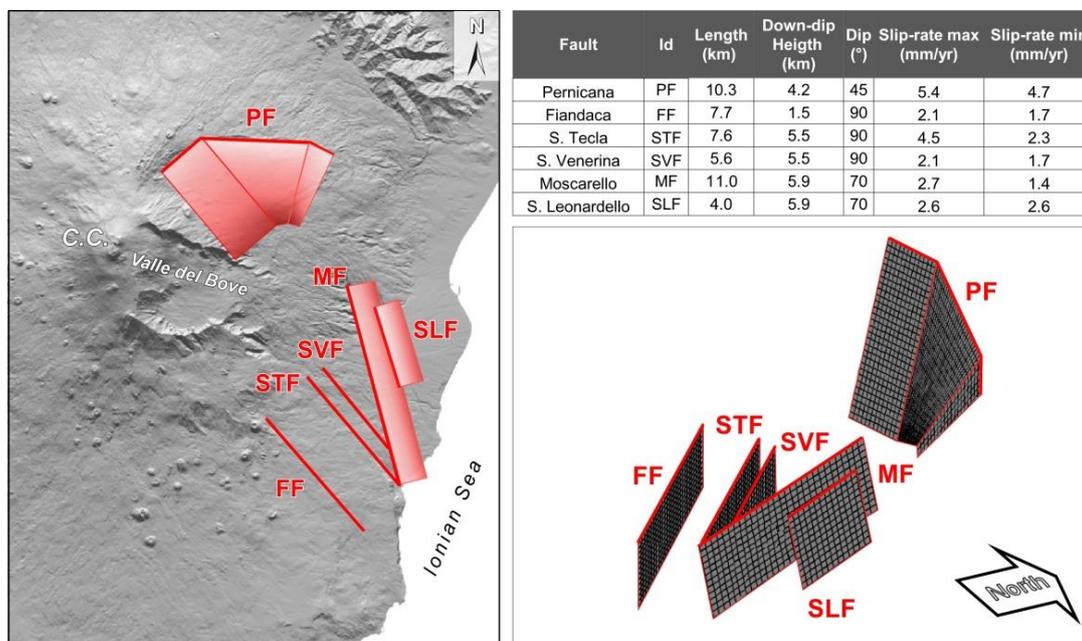
Figure 9: Pattern of individual sources used in the geological model and related geometric-kinematic parameters: red boxes in the left frame represent the projection at the surface of the fault planes, lines indicate the vertical planes. Note that lengths refer to the seismogenic fault segments only, whereas the ones governed by prevailingly creeping behaviour are not considered.

610
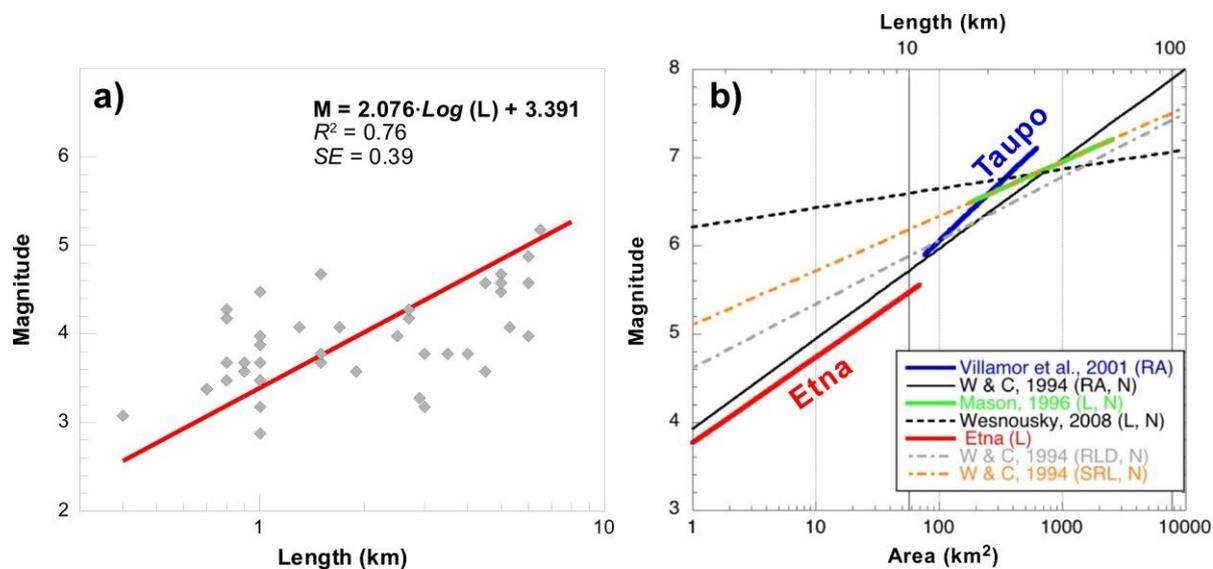
Figure 10: a) Plot of earthquake magnitude vs rupture length for the Etna region (this study); b) Comparison with the magnitude-size scaling relationships for the Taupo volcanic zone (Villamor et al., 2001) and other worldwide relationships (Wells and Coppersmith, 1994; Mason, 1996; Wesnousky, 2008). Abbreviations: L, fault length; N, normal kinematics; RA, rupture area; RLD, rupture length at depth; SRL, surface rupture length.

615

620
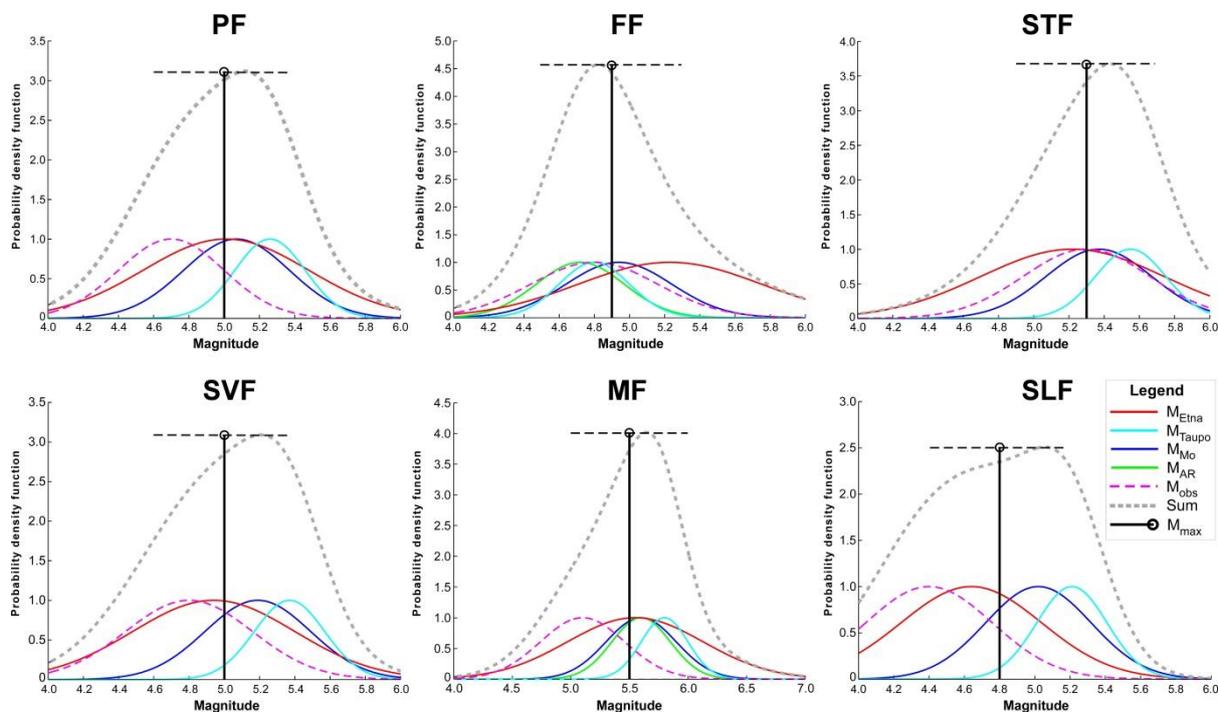
Figure 11: Maximum magnitudes (M$_{max}$) estimated by the *FiSH* code for the studied faults. Abbreviations: M$_{Etna}$-M$_{Taupo}$, magnitude from earthquake scaling relationships for Etna and Taupo; M$_{Mo}$, scalar seismic moment magnitude; M$_{AR}$, magnitude from aspect ratio relationships; M$_{obs}$, maximum observed magnitude. Uncertainties are represented by probability curves (see text for explanation).